



Research Article

Exergetic efficiency prediction of roughened solar air heater

KARMVEER¹, Naveen Kumar GUPTA^{1,*}, Tabish ALAM², Himanshu SINGH³

¹Institute of Engineering and Technology, GLA University, Mathura, 281406, India

²CSIR-Central Building Research Institute, Roorkee, 247667, India

³Invertis University, Bareilly, 243112, India

ARTICLE INFO

Article history

Received: 02 February 2022

Revised: 29 May 2022

Accepted: 02 June 2022

Keywords:

Roughness; Exergetic Efficiency; Thermal Efficiency; Solar Air Heater; Nusselt Number

ABSTRACT

Energy losses of flowing air through solar air heater (SAH) duct does not consider in the thermal performance. Therefore, thermohydraulic performance based on exergetic efficiencies is a tool to assess the performance by considering energy losses in propelling the air simultaneously to identify the best ribs configuration. This paper presents the thermohydraulic performance of SAHs exploiting various ribs roughness's. The performance of SAHs is based exergetic evaluation based on IInd law of efficiency is most suitable for design of artificially roughened SAH as it includes both requirement of pumping power and effective energy output. In this paper exergetic evaluation of differently roughened SAH has been done. The exergy efficiency of roughened SAH was calculated analytically with the help of correlations developed by researchers and the results also compared with conventional SAH under same operating parameters. The thermal and exergy efficiency curve as a function of temperature rise parameter ($\Delta T/I$) has been plotted. As a results, hybrid ribs configuration exhibited the highest exergetic efficiencies when temperature rise parameters greater than 0.01 K.m/W, however, smooth duct also showed a significant exergetic efficiency when temperature rise parameters had low values.

Cite this article as: Karmveer, Gupta NK, Alam T, Singh H. Exergetic efficiency prediction of roughened solar air heater. J Ther Eng 2023;9(3):718–732.

INTRODUCTION

The energy demand increasing day-by-day globally because of rapid growth in population and industrialization due to which world fossil fuel reserve depletes drastically. Also, power generation from fossil fuels causes environmental degradation. Hence there is a need to shift from convention fuels- towards the non-conventional energy resources. Among available renewable energy sources solar

energy is the freely available, easily accessible, cost effective, clean and inexhaustible source of energy. So, solar energy has great potential to strengthen industrialization and economic development. Solar energy will be the solution of future energy crises. The effective and adequate utilization of solar energy leads to amelioration in social, economic and environmental aspects of any nation. In the thermal route of solar energy application, the solar air heater

*Corresponding author.

*E-mail address: naveen.gupta@gla.ac.in

This paper was recommended for publication in revised form by Regional Editor Ahmet Selim Dalkılıç



(SAH) is used to convert solar energy into thermal energy. Generally, it is used for low grade thermal energy applications [1, 2]. The design of SAH is very simple, maintenance free and cheap. The efficiency of SAH is poor due to lesser value of convective coefficient in between absorber plate and flowing air. The heat transfer can be enhanced by using roughness in the SAH duct [3, 4]. The roughness may be of distinct shape and size [5-7].

Sahu and Prasad [8] studied performance of arc shape protrusions using exergetic efficiency. They suggest that at Re higher than 20000 the conventional smooth SAH is suitable because at higher Re exergy of thermal energy collected by SAH fall behind the value of exergy of required pumping power. Singh et al. [9] studied discrete-V-down rib roughened SAH using exergy analysis. The exergy analysis based on second law incorporates required pumping power and output energy. The highest amount of energy that can be obtained from a particular type of energy is called exergy [10, 11]. The analysis based on second law of efficiency of rib roughened SAH has been reported by Kumar et al. [12], Gupta and Kaushik [13–15] and Layek et al. [16]. Kumar et al. [12] studied performance of winglet type roughness roughened absorber surface of SAH by using exergy analysis. Kaushik and Gupta [13, 14] did thermo-hydraulic performance evaluation of SAH with the help of thermal, exergetic and effective efficiencies. They reported that for the optimum value of aspect ratio of collector and duct height there will be an optimal value of number of glass cover (M) for a particular application. For higher value of M low aspect ratio of collector and higher duct depth will give higher exergetic efficiency and in case of lower value of M high aspect ratio of collector and low duct height will give higher value of exergetic efficiency. They reported that circular and V-shaped rib shows appreciable value of exergy efficiency in the higher range of Re. Gupta and Kaushik [15] studied performance of expanded metal-mesh type of roughness. They carried out performance evaluation in terms of effective and exergy energy enhancement ratio at distinct value of Re. The enhancement ratios increase with the increase in I and duct depth. They reported that exergy enhancement ratio is a meaningful criterion for SAH performance evaluation. Layek et al. [16] studied numerically entropy generation in chamfered rib groove type of roughness in repeated manner. The set of parameter relative pitch ratio (p/e) = 6, relative groove position (g/p) = 0.4 and chamfer angle (ϕ) = 18° shows minimum rise in entropy generation.

Momin et al. [17] experimentally studied performance of V-shape rib roughened SAH. The parameter relative rib height (e/D_h), angle of attack (α) and Reynolds number (Re) varies as 0.02-0.034, 30-90° and 2500-18000 respectively whereas p/e = 10. They reported that the Nu enhances by 1.14 times more as comparison to inclined ribs at Re = 17034. The highest augmentation in Nu and f were 2.30 and 2.83 times at α = 60°. They also reported that the effect of Re on Nu is much stronger as that of α . Istanto et al. [18] studied performance of continuous ribs of V-down shape

roughened SAH duct. The Re varies from 3500 to 10000. Highest value of thermal performance has been achieved at α = 60°. Singh et al. [19, 20] studied performance of V-shape down discrete rib roughness. The parameter α , relative gap width (g/e), relative gap position (d/w), Re, e/D_h and p/e varies as 30°-75°, 0.5-2.0, 0.20-0.80, 3000-15000, 0.015-0.043 and 4-12 respectively. Deo et al. [21] studied performance of V-down shape rib combine with staggered rib with multi gap roughened SAH duct. The experimental parameters e/D_h , α , Re and p/e ranges as 0.026 - 0.057, 40° - 80°, 4000 - 12000 and 4 - 14 respectively. The value of fixed parameter staggered rib length to rib height ratio (w/e), g/e and relative staggered rib pitch (P/p) 4.5, 1 and 0.65 respectively. Hans et al. [22] studied performance of multi-V-shaped rib roughness. The experimental parameter Re, e/D_h , W/w , α and p/e varies as 2000-20000, 0.019-0.043, 1- 10, 30° - 75°, and 6 -12 respectively. They maximum augmentation in Nu and f occurs at p/e = 8. Singh et al. [23] studied multi V-shaped ribs with uniform gap roughened SAH duct. The f and Nu were increased by 5.67 and 6.46 at W/w =6. Kumar et al. [24, 25] studied V-shape rib roughness with parameters W/e , e/D_h , g/e , W/w , p/e , and d/x equals to 12, 0.0433, 1.0, 6, 10 and 0.69 respectively. The value of α varies from 30-75°. They Nu has highest value at α = 60°.

Yadav et al. [26] studied performance of circular-protrusion type of roughness. The study parameter arc angle (α') and Re varies as 45°- 75° and 3600 – 18100 respectively. The maximum increment Nu is 2.89 times at α' equals to 60°. Hans et al. [27] studied performance of broken arc rib type of roughness. The broken arc contains uniform gaps. The experimental parameter g/e , d/w , p/e , α' , e/D_h and Re varies as 0.5 -2.5, 0.5 - 0.8, 4 - 12, 15-75°, 0.022-0.043 and 2000 to 16000 respectively. They reported that the Nu enhanced by 2.63 times at e/D_h = 0.043. Gill et al. [28] studied performance of hybrid-rib roughness. The study parameter e/D_h , α' , and Re varies as 0.022-0.043, 15-75°, and 2000-16000 respectively. The Nu was enhanced by 3.16 times at e/D_h equals to 0.043. Lanjewar et al. [29] studied W-shape rib roughness both in W-down and W-up pattern type of roughness. The parameter e/D_h = 0.03375 and Re equal to 2300 -14000. The W-down pattern has better performance as that of W-up pattern. The highest value of thermohydraulic ratio for W-up and W-down patterns is 1.73 and 1.95 respectively. Kumar et al. [30] studied effect of discrete-W-shape rib roughness. The value of parameter p/e = 10 and α = 30° to 75°, e/D_h varies from 0.0168 to 0.0338. Nu enhances with the increase in the value of Re. Gawande et al. [31] studied performance of reverse L-shape repeated roughness. The experimental parameter p/e and Re varies as 7.14 - 17.86 and 3800-18000 respectively. The THPP was found in the range of 1.92 to 1.90.

Kumar and Layek [32, 33] studied performance of winglet types of turbulators with small hole at tip. The experimental parameter varies as α = 30° - 75°, W/w = 3 - 7 and Re = 3000 - 22000. Patel et al. [34] studied performance of reverse-NACA 0040 profile rib roughness. The parameter

p/e and e/D_h equal to 8 and 0.065 respectively. Kumar and Layek [35] also have done exergetic performance evaluation for the above roughness. Promvong et al. [36] experimentally studied performance of V-shape ribs and delta-groove roughness. The parameter $Re = 7000 - 30000$. Hans et al. [37] studied performance of broken arc ribs. The experimental parameter p/e , g/e , e/D_h and α varies as 4-12, 0.5-2.5, 0.2-0.8, and 15° - 75° respectively. Al-Dulaimi et al. [38] studied performance of rectangular turbulators in a square duct. The thermal performance augmented remarkably. Afsharpanah et al. [39] studied performance of multi-twisted tape insert type of roughness. Sachdeva et al. [40] studied performance of U-shape fin by placing longitudinally in the duct. The air outlet temperature decreased by 25°C as flowing rate of air increased from 40 kg/hr to 180 kg/hr. The detailed review of different artificial roughness of distinct shape and size used in SAH have been presented in the past [41, 42].

The literature shows that various rib configuration has been investigated experimentally. The results have been presented in term of Nu , f and thermal performance and these parameters have been compared individually. Also, it has been found that those ribs configuration which have high Nusselt number, also have high friction factor (higher air Pm). So, it is become necessary to mutual consideration of Nusselt number and friction factor to assess the most advantageous configuration. Therefore, exergetic efficiency of various rib configuration have been evaluated considering Nu and f . Also, exergetic efficiency of various ribs configurations have been compared with smooth duct. In view of above, the present study is carried out to meet out the following objective: to study the exergetic efficiency characteristics distribution for various ribs configuration and compared with exergetic efficiency with conventional smooth absorber in SAH. Also, best ribs configuration have been identify which provide maximum exergetic efficiency.

THERMAL AND EFFECTIVE PERFORMANCE ASSESSMENT APPROACH OF ROUGHENED SAH

The useful heat gain (Q_u) can be evaluated as [43],

$$Q_u = [I(\tau\alpha)_{avg} - U_o(T_{pm} - T_a)]A_p \quad (1)$$

where,

$(\tau\alpha)_{avg}$ - product of transmittance and absorbance

U_o - overall heat loss coefficient,

T_{pm} - absorbing plate mean temperature

T_a - ambient temperature

A_p - Absorber plate area.

The overall heat loss coefficient [43],

$$U_o = U_t + U_b + U_e \quad (2)$$

where,

U_b - back loss coefficient

U_e - edge loss coefficient

U_t - top loss coefficient

$$q_{loss,p-c} = h_{c,c-p}(T_p - T_c) + \frac{\sigma(T_p^4 - T_c^4)}{\frac{1}{\epsilon_p} + \frac{1}{\epsilon_c} - 1} = (h_{c,p-c} + h_{r,p-c})(T_p - T_c) \quad (3)$$

$$\text{where, } h_{r,p-c} = \frac{\sigma(T_p^2 + T_c^2)(T_p + T_c)}{\frac{1}{\epsilon_p} + \frac{1}{\epsilon_c} - 1} \quad (4a)$$

$$R_2 = \frac{1}{(h_{c,c-p} + h_{r,c-p})} \quad (4b)$$

Heat transfer due to convection between absorber plate and glass cover,

$$h_{c,p-c} = \frac{Nu.k}{L} \quad (5)$$

Heat transfer due to radiation between sky and glass cover,

$$h_{r,c-a} = \frac{\sigma\epsilon_c(T_c + T_s)(T_c^2 + T_s^2)(T_c - T_s)}{(T_c - T_a)} \quad (6)$$

The resistance to ambient,

$$R_1 = \frac{1}{(h_{r,c-a} + h_w)} \quad (7)$$

The top loss coefficient from glass cover to the surrounding is,

$$U_t = \frac{1}{(R_1 + R_2)} \quad (8)$$

The edge loss coefficient is,

$$U_e = \frac{1}{R_4} = \frac{(UA)_{edge}}{A_p} \quad (9)$$

The back loss coefficient is,

$$U_b = \frac{1}{R_3} = \frac{k_{ins}}{T_i} \quad (10)$$

The thermal efficiency is,

$$\eta_{th} = \frac{Q_u}{A_p I} \quad (11)$$

The net effective efficiency is expressed as [44],

$$\eta_{net} = \frac{Q_u - \frac{P_m}{C}}{A_p I} \quad (12)$$

where, C (=0.18) is a conversion factor used for to convert P_m in to thermal energy. P_m is the required mechanical power by blower for propelling air. The P_m can be expressed as[45],

$$P_m = \frac{m \cdot \Delta P_d}{\rho_a} \quad (13a)$$

Where, ΔP_d is the pressure drop. The ΔP_d can be expressed as [34],

$$\Delta P_d = \frac{4f \cdot L \cdot \rho_a \cdot V^2}{2d_h} \quad (13b)$$

The exergetic efficiency can be defined as the ratio of net exergy flow rate to the air (E_n) and exergy related with solar irradiation (E_s). Altified et al. [54] suggested following exergy loss components-

- a) Exergy losses by friction.
- b) Exergy losses due to optical losses.
- c) Exergy losses due to absorption of irradiation.
- d) Exergy losses due to transferring of heat to the flowing air.
- e) Exergy losses from absorber surface to the environment.

MATHEMATICAL MODEL FOR EXERGETIC PERFORMANCE EVALUATION OF SAH

The calculation of thermal and exergetic efficiency of SAH proceeds by using value of parameters. The range of system parameter based on various experimental studies and operating parameters decided on the basis of application. The optimum thermal and exergetic efficiency has been calculated by using solar insolutions (I) and $\Delta T/I$. The distinct properties of air i.e. dynamic viscosity (μ), density (ρ) thermal conductivity (k) and specific heat (C_p) were calculated with the help of relations given by Bhushan and Singh [46] and Hans [47] and as,

$$\mu = 1.81 \times 10^{-5} \times \left(\frac{T_f}{293} \right)^{0.735} \quad (14)$$

$$\rho = \left(\frac{P_a}{RT_f} \right) \quad (15)$$

$$k = 0.0275 \times \left(\frac{T_f}{293} \right)^{0.086} \quad (16)$$

$$C_p = 1006 \times \left(\frac{T_f}{293} \right)^{0.0155} \quad (17)$$

Table 1. Value/range of parameters.

Parameter	Value/Range
System Parameters	
<i>Fixed</i>	
Collector duct height (H), m	0.025
Collector length (L), m	1.0
Collector width (W), m	0.3
Emissivity of absorber plate (ϵ_p)	0.9
Emissivity of transparent glass cover (ϵ_g)	0.88
Gap between collector and glass cover (L_g)	0.025
Number of glass cover (N)	1
Thickness of back insulation (t_i), m	0.05
Thermal conductivity of insulation (k_i), W/m.K	0.037
Thickness of collector edge (t_c), m	0.1
Thickness of glass cover (t_g), m	0.002
Tilt angle (β_{ti})	30°
Transmittance-absorptance product	0.8
<i>Variable</i>	
Relative rib height (e/D_h)	0.020-0.044
Relative rib pitch (p/e)	6-12
Operating parameters	
<i>Fixed</i>	
Ambient temperature (T_a), K	285
Wind velocity (V_w), m/s	1.0
<i>Variable</i>	
Insolation (I), W/m ²	600 - 1000
Temperature rise parameter ($\Delta T/I$), K.m ² /W	0.002 - 0.030

The procedure adopted for calculation of thermal and effective efficiency is same as it was given by Alam et al.[44] and a Matlab code has been generated for the same. The calculation procedure of thermal and exergetic efficiency as suggested by Singh et al. [5], Yadav and Kaushal [48], Alam et al. [49], Sahu and Prasad [50], Chamoli and Thakur [51], and Karmveer [52, 53] is as follows:-

Step 1: Firstly, Initialize values of fixed system and operating parameter from Table1.

Step 2: The outlet temperature (T_o) of the air is calculated as,

$$T_o = \left(\frac{\Delta T}{I} \right) \times I + T_i \tag{18}$$

The inlet temperature of air is considered to be same as surrounding temperature.

Step 3: The mean fluid temperature calculated as,

$$T_{mf} = \frac{T_o + T_i}{2} \tag{19}$$

Step 4: The value of mean plate temperature presumed as,

$$T_{mp} = \frac{(T_o + T_i)}{2} + 10 \tag{20}$$

Step 5: The thermo physical properties of air are calculated with the help of correlation 14, 15, 16 and 17 given by Bhushan and Singh [46] and Hans [47].

Step 6: The overall heat loss coefficient (U_o) is calculated as given in equation 2.

Where, the top heat loss coefficient is calculated as [45],

$$\frac{1}{U_i} = \left[\frac{\sigma(T_{pm}^2 + T_o^2)(T_{pm} + T_o)}{\left(\frac{1}{\epsilon_p} + \frac{1}{\epsilon_g} - 1 \right)} + \left(\frac{k_i Nu_i}{L_g} \right) \right]^{-1} + \left[\sigma \epsilon_g (T_g^2 + T_o^2)(T_g + T_o) + h_w \right]^{-1} + \frac{t_g}{k_g} \tag{21a}$$

where,

$$T_g = \left(\frac{F_i T_{pm} + c T_a}{I + F_i} \right)$$

where,

$$T_g = \left(\frac{F_i T_{pm} + c T_a}{I + F_i} \right)$$

where,

$$F_i = \frac{[12 \times 10^{-8} (T_o + 0.2 T_p)^3 + h_w]^{-1} + 0.3 t_g}{[6 \times 10^{-8} (\epsilon_p + 0.028) (T_{pm} + 0.5 T_o)^3 + 0.6 L_g^{-0.2} \{ (T_{pm} - T_o) \cos \beta_{ii} \}^{0.25}]^{-1}}$$

$$c = \left[\frac{(T_s / T_a) + (h_w / 3.5)}{I + h_{w+3.5}} \right]$$

$$T_s = 0.0522 (T_a)^{1.5}$$

$$Nu_i = 1 + 1.44 [1 - 1708 / Ra \cos \beta_{ii}]^+ \{ [1 - 1708 (\sin 1.8 \beta)^{1.6} / Ra \cos \beta_{ii}] + [(Ra \cos \beta_{ii} / 5830)^{0.33} - 1] \}$$

$$Ra = Gr \times Pr$$

$$\text{and, } G_r = \frac{g \beta' (T_m - T_g) L_g^3}{\nu^2}$$

The back cover heat loss coefficient is calculated as,

$$U_b = \frac{k_{ins}}{T_i} \tag{21b}$$

The edge heat loss coefficient is calculated as,

$$U_e = \frac{(L + W) t_e k_i}{L W t_i} \tag{21c}$$

Step 7: The useful heat gain is calculated as,

$$Q_{ul} = [I(\tau \alpha) - U_o (T_{pm} - T_a)] A_p \tag{22}$$

Step 8: The mass flow rate is calculated as,

$$m = \frac{Q_{ul}}{C_p \Delta T} \tag{23}$$

Step 9: The Reynolds number is calculated as,

$$Re = \frac{m D_h}{\mu W H} \tag{24}$$

Step 10: The Nusselt number of different roughness surfaces have been estimated with help of their developed correlations. Then convection coefficient of heat transfer has been estimated as,

$$h = \frac{Nu.k}{D_h} \tag{25}$$

The Nu for smooth surface has been estimated with the help of Dittus-Boelter correlation as,

$$Nu = 0.023 Pr^{0.4} Re^{0.8} \tag{26}$$

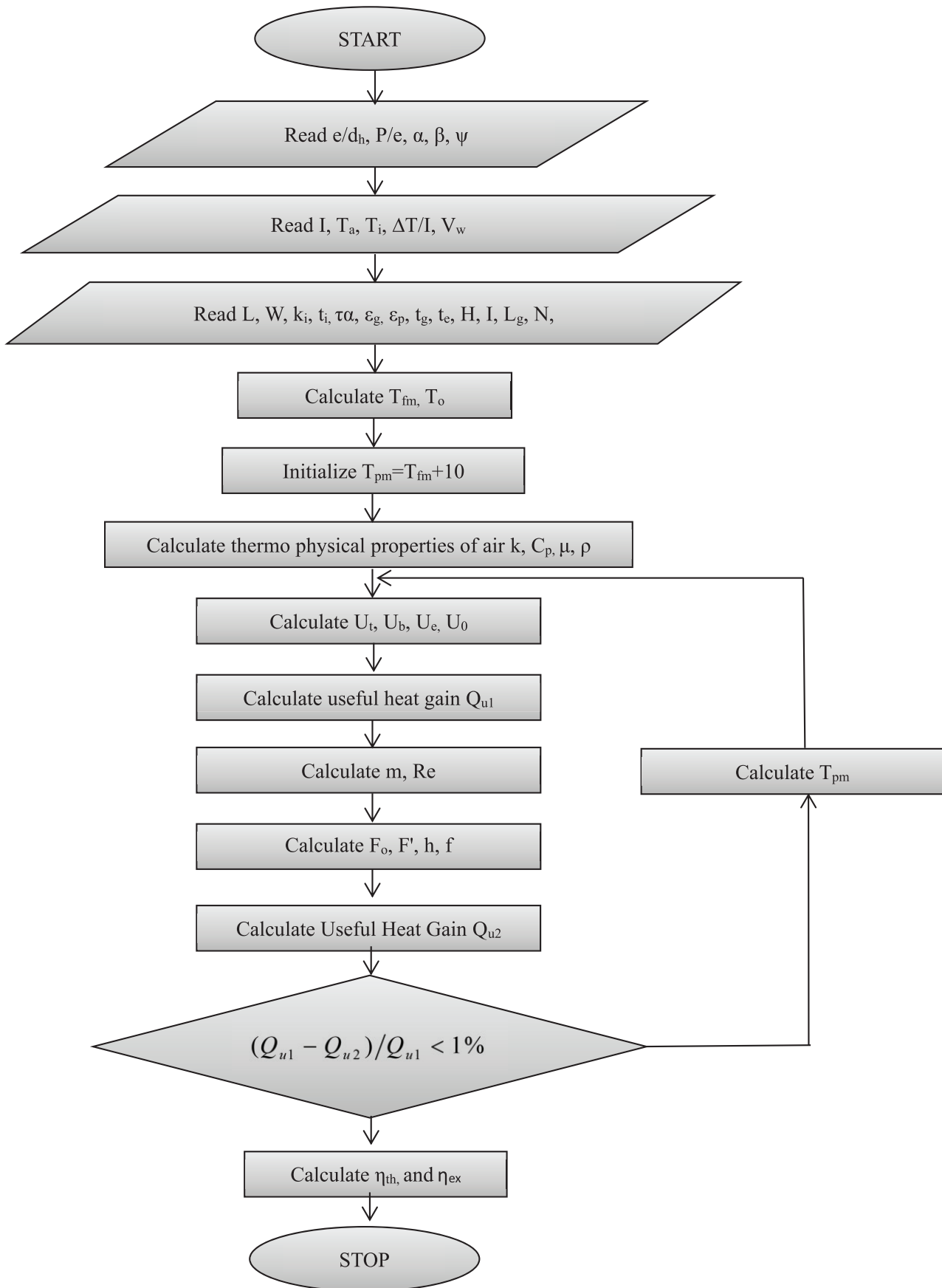


Figure 1. Flow chart of methodology

$$Q_{u2} = A_p F_o [I(\tau\alpha) - U_l(T_o - T_a)] \quad (27)$$

where,

$$F_o = \frac{mC_p}{A_p U_l} \left[\exp \left\{ \frac{F' A_p U_l}{mC_p} \right\} - 1 \right]$$

$$F' = \frac{h}{h + U_o}$$

Step 12: Then, Q_{u1} and Q_{u2} are compared if, these values are not matched with each other, the new value of T_{pm} is determined by using the value of heat gain, Q_{u2} , from the eq. 23. Iteration continues until the values of Q_{u1} and Q_{u2} ,

comes close enough $\left(i.e. \frac{Q_{u1} - Q_{u2}}{Q_{u1}} < 1\% \right)$.

$$T_{pm} = T_a + \left[\frac{I(i\alpha) - Q_{u2}/A_p}{U_l} \right] \quad (28)$$

Step 11: Again, heat gain by the flowing air is evaluated as follows [43];

Step 13: The friction factor of different roughness surfaces has been estimated with help of their developed correlations. The friction factor of smooth surface has been estimated with the help of Blasius correlation as [13],

$$f = 0.079 \text{Re}^{-0.25} \quad (29)$$

Step 14: The Pm is calculated with help of equation 13a.

Step 15: The ΔP_d has been calculated with the help of equation 13b.

Step 16: The exergy efficiency is calculated as,

$$\eta_{ex} = \frac{E_n}{E_s} \quad (30)$$

It can be maximized and minimized by increasing and decreasing the value of E_n and E_s .

where,

E_n - Net exergy flow rate to the air

E_s - Exergy related with solar irradiation

E_n can be expressed as;

$$E_n = IA_p \eta_{th} \eta_c - P_{pd}(1 - \eta_c)$$

where,

I- Intensity of global radiation

P- Pumping power

η_c - Carnot efficiency $(1 - T_a/T_{fm})$

E_s can be expressed as [54];

$$E_s = I \left(1 - \frac{T_a}{T_s} \right)$$

Where, T_s is the surface temperature of the sun, its value considered as 5762 K.

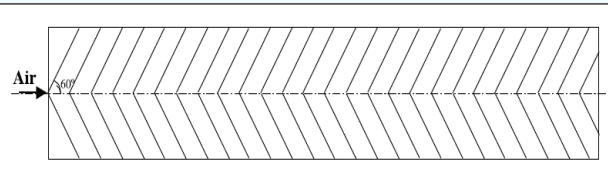
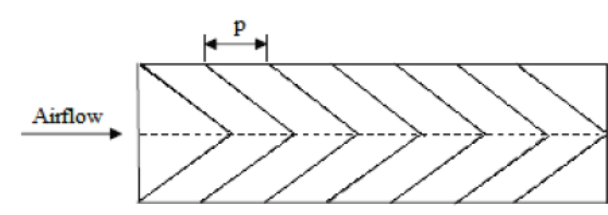
Step 17: Finally, thermal efficiency, effective efficiency and exergetic efficiency of different roughness has been estimated.

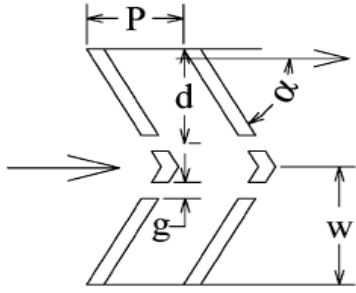
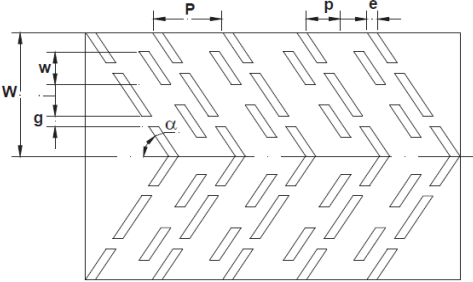
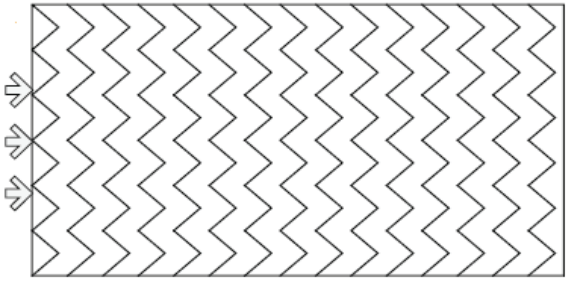
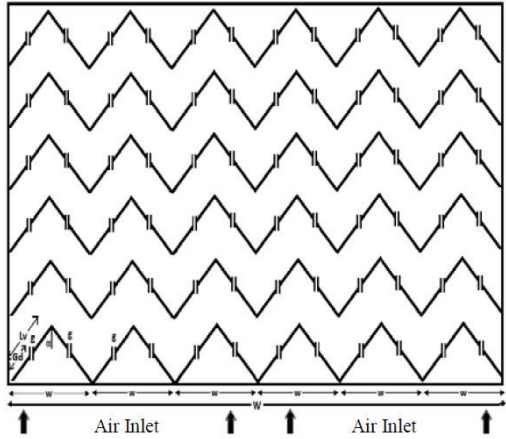
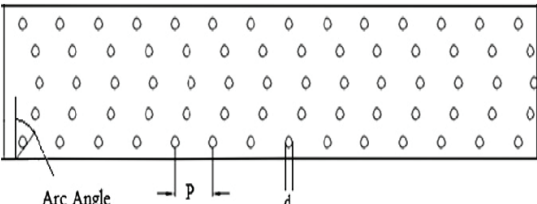
The flow chart of the mathematical model is shown in Figure 1.

DISCUSSION

The numerical analysis with different type of roughness geometry, shape and arrangements is carried out with the help exergetic evaluation of roughened duct of SAH. The system and operating parameter with various type of roughness geometry and their arrangements are considered for evaluating exergetic performance of SAH. The parameters of exergetic evaluation are tabulated in Table 1. The investigated distinct roughness geometries against the smooth duct shown in Table 2.

Table 2: Investigated roughness geometries against the smooth SAH.

Investigators	Type of roughness	Shape and geometry	Roughness figure
Ebrahim-Momin et al. [17]	Wired artificial roughness	V-shaped ribs	
Istanto et al. [18]	Wired artificial roughness	V-down continuous ribs	

<p>Singh et al. [19]</p>	<p>Wired artificial roughness</p>	<p>Discrete V-down ribs</p>	 <p>A schematic diagram of discrete V-down ribs. It shows a top-down view of a channel with several V-shaped ribs pointing downwards. The distance between the centers of two adjacent ribs is labeled P. The height of a rib is labeled d. The angle of the rib's side is labeled α. The gap between the ribs is labeled g. The total width of the channel is labeled W. Arrows indicate the flow direction from left to right.</p>
<p>Deo et al. [21]</p>	<p>Wired artificial roughness</p>	<p>Multi-gap-V-down ribs</p>	 <p>A schematic diagram of multi-gap-V-down ribs. It shows a top-down view of a channel with a grid of V-shaped ribs. The distance between the centers of two adjacent ribs is labeled P. The width of a rib is labeled p. The gap between ribs is labeled e. The height of a rib is labeled w. The gap between the ribs is labeled g. The angle of the rib's side is labeled α. Arrows indicate the flow direction from left to right.</p>
<p>Hans et al. [22]</p>	<p>Wired artificial roughness</p>	<p>Multiple V-ribs</p>	 <p>A schematic diagram of multiple V-ribs. It shows a top-down view of a channel with a continuous zigzag pattern of V-shaped ribs. Arrows on the left side indicate the flow direction from left to right.</p>
<p>Kumar et al. [24]</p>	<p>Wired artificial roughness</p>	<p>Multiple V-ribs with gap</p>	 <p>A schematic diagram of multiple V-ribs with gap. It shows a top-down view of a channel with a grid of V-shaped ribs. The height of a rib is labeled w. The distance between the centers of two adjacent ribs is labeled p. The gap between ribs is labeled g. Arrows at the bottom indicate the flow direction from left to right, with labels "Air Inlet".</p>
<p>Yadav et al. [26]</p>	<p>Protrusion</p>	<p>Circular protrusions</p>	 <p>A schematic diagram of circular protrusions. It shows a top-down view of a channel with a grid of small circles. The distance between the centers of two adjacent circles is labeled P. The diameter of a circle is labeled d. The angle of the protrusion is labeled "Arc Angle". Arrows at the bottom indicate the flow direction from left to right.</p>

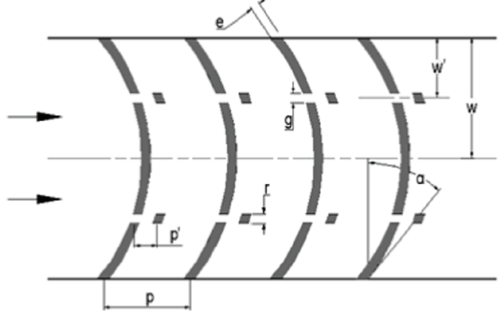
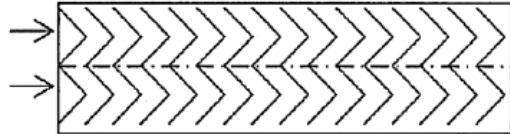
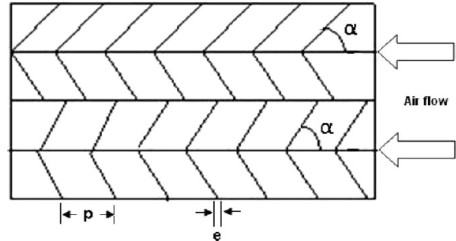
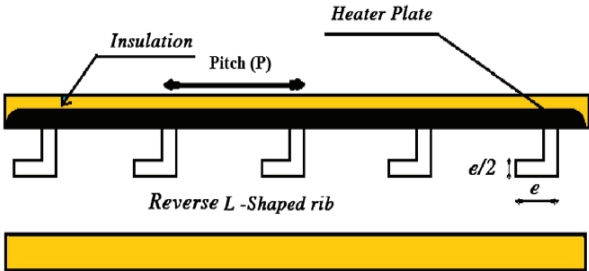
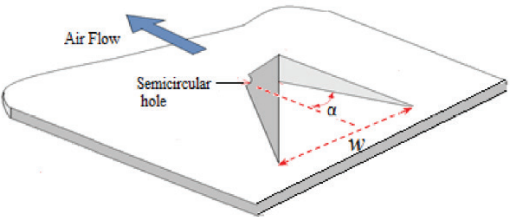
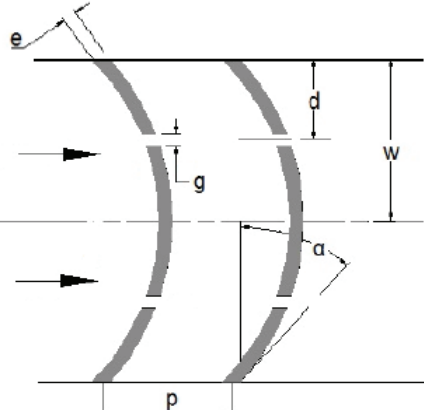
<p>Gill et al. [28]</p>	<p>Wired artificial roughness</p>	<p>Broken arc with staggered rib</p>	
<p>Lanjewar et al. [29]</p>	<p>Wired artificial roughness</p>	<p>W-shaped ribs</p>	
<p>Kumar et al. [30]</p>	<p>Wired artificial roughness</p>	<p>Discrete W- shaped ribs</p>	
<p>Gawande et al. [31]</p>	<p>Obstacle</p>	<p>L-shaped rib</p>	
<p>Kumar and Layek [33]</p>	<p>Turbulator</p>	<p>Winglet type</p>	
<p>Hans et al. [37]</p>	<p>Wired artificial roughness</p>	<p>Broken arc ribs</p>	

Table 3. Exergetic efficiency data at distinct value of $\Delta T/I$

$\Delta T/I$	0.002	0.004	0.006	0.008	0.01	0.012	0.014	0.016	0.018	0.02	0.022	0.024	0.026	0.028	0.03
Smooth	-0.01162	0.00325	0.0065	0.00842	0.00984	0.01082	0.01154	0.01201	0.01223	0.01209	0.01188	0.01152	0.01088	0.01026	0.00958
Momin et al. [17]	-0.02448	0.00123	0.00641	0.0093	0.01143	0.0132	0.01469	0.01593	0.01694	0.01756	0.01808	0.01837	0.01847	0.01818	0.01784
Ishanto et al. [18]	-0.03627	-0.00228	0.00502	0.00881	0.01156	0.01383	0.01568	0.01735	0.0188	0.02006	0.02112	0.02201	0.02273	0.02305	0.02337
Singh et al. [19]	-0.04873	-9.29E-04	0.00613	0.00958	0.01213	0.0143	0.01622	0.01778	0.01926	0.02055	0.02168	0.02262	0.02341	0.02403	0.02424
Deo et al. [21]	-0.04478	-6.56E-04	0.00638	0.00998	0.01274	0.01514	0.01734	0.01936	0.02123	0.02296	0.02455	0.0258	0.02706	0.02817	0.02914
Hans et al. [22]	-0.04209	-0.00559	0.00468	0.00926	0.01247	0.01524	0.01758	0.01981	0.02189	0.02384	0.02567	0.02739	0.02899	0.03049	0.03188
Singh et al. [23]	-0.04482	-0.00205	0.00567	0.00955	0.01236	0.01472	0.01678	0.01847	0.01998	0.02125	0.02227	0.02285	0.02325	0.02334	0.02285
Kumar et al. [24]	-0.04895	-0.0066	0.00436	0.00914	0.01241	0.01521	0.0176	0.01985	0.02194	0.02391	0.02576	0.02748	0.0291	0.03061	0.03201
Yadav et al. [26]	-0.01561	0.00236	0.00704	0.01007	0.01259	0.01482	0.01683	0.01867	0.02017	0.02159	0.02282	0.02387	0.02473	0.02541	0.02565
Gill et al. [28]	-0.04008	-0.02273	-0.00335	0.00885	0.01107	0.01465	0.01759	0.02013	0.02258	0.0249	0.0269	0.02887	0.03073	0.03248	0.03412
Lanjewar et al. [29]	-0.02809	0.00132	0.00656	0.0094	0.01149	0.01323	0.01468	0.01588	0.01684	0.01738	0.01781	0.01802	0.01784	0.01757	0.01709
Kumar et al. [30]	-0.02815	6.91E-04	0.00638	0.0095	0.0119	0.01395	0.01561	0.01715	0.01849	0.01964	0.0206	0.0214	0.02183	0.02223	0.02246
Gawande et al. [31]	-0.047	-0.00135	0.0059	0.00952	0.01222	0.01452	0.01658	0.01847	0.0202	0.02162	0.02302	0.02428	0.0254	0.02639	0.02726
Kumar et al. [33]	-0.03699	-4.89E-04	0.00603	0.00934	0.01178	0.0137	0.01536	0.01677	0.01794	0.01888	0.01941	0.01983	0.02003	0.02002	0.01953
Hans et al. [37]	-0.03535	7.12E-04	0.00659	0.0097	0.01206	0.01394	0.01557	0.01693	0.01803	0.0187	0.0192	0.01942	0.01913	0.01868	0.01769

The thermohydraulic performance of SAH does not take into account the various energy losses in propelling the air through duct of SAH. The exergetic evaluation based on IInd law of efficiency is most suitable for design of artificially roughened SAH. In this paper an attempt has been made for exergetic evaluation of distinct type of roughness's used by various researchers. The exergetic efficiency of distinct type of roughness's evaluated numerically by using correlations

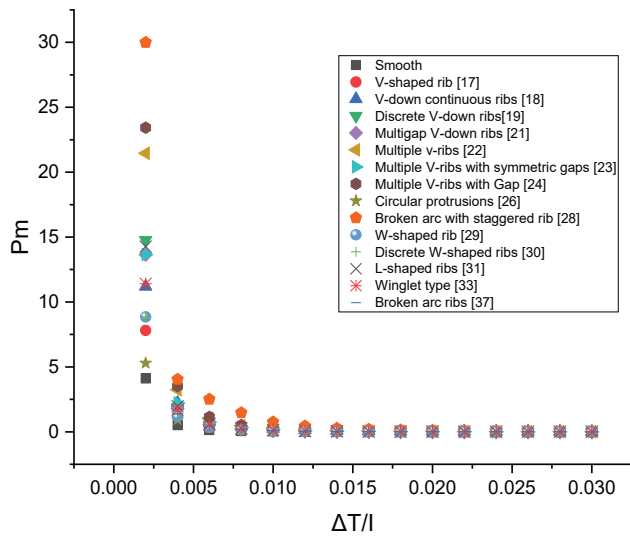


Figure 2. Pm of roughened duct with respect to $\Delta T/I$.

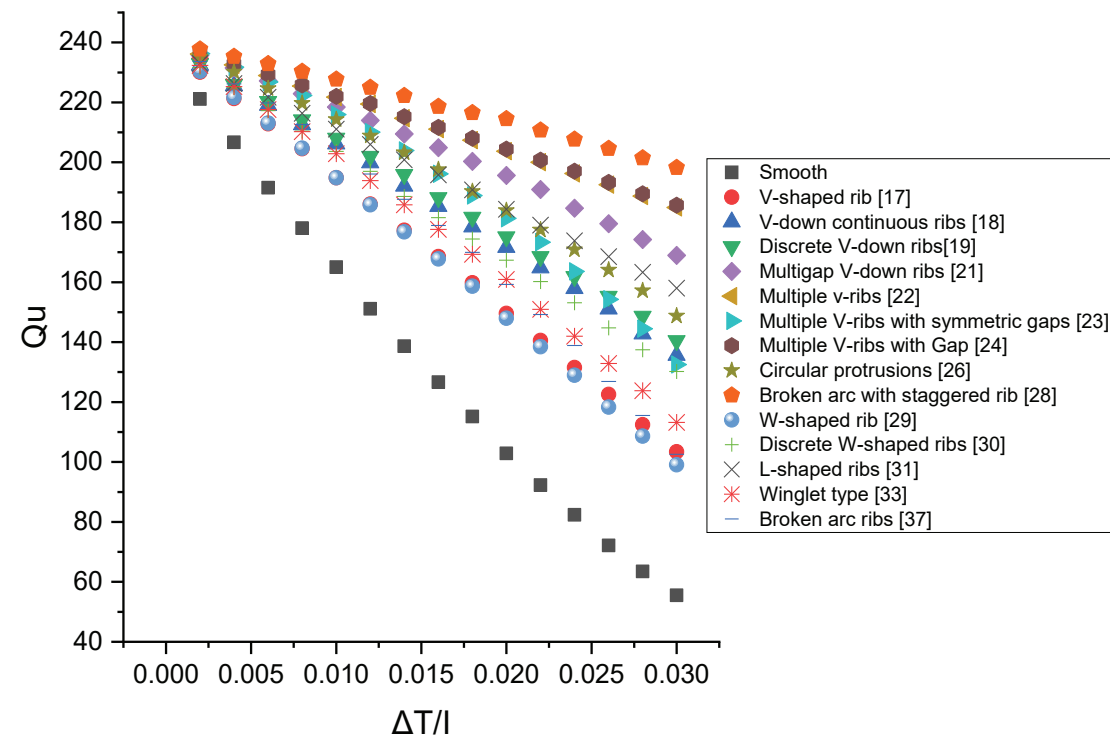


Figure 3. Qu of roughened duct with respect to $\Delta T/I$.

of Nu and f developed by respective researchers and results of these roughness's compared with smooth SAH duct.

The exergy efficiency is evaluated by using the methodology discussed above for distinct operating parameters of roughened SAH. It is found that the roughened surface of absorber plate remarkably augments the efficiencies as that of smooth surface. The staggered broken-arc hybrid rib shows consistently higher value of η_{thermal} over the other roughness's.

The pumping power required due to various ribs including conventional smooth absorber has been plotted as a function of temperature rise parameters as shown in Figure 2. It can be seen that pumping power due to all ribs configurations decrease at very fast rate at lower temperature rise parameter value, thereafter, pumping power requirement become stagnant at higher temperature rise parameters. Also, pumping power requirement for broken arc with staggered ribs [28] is found to be higher in comparison to other ribs configurations, however, this difference is not significant at higher temperature rise parameter. Similarly, heat gain due to various ribs configuration have been plotted as a function of temperature rise parameter as shown in Figure 3. The useful heat gain of all rib's configuration decrease with increase in temperature rise parameters. The maximum heat gain is found in case of broken arc with staggered ribs [28] which decrease 240 to 210 watts when temperature rise parameter vary from 0.002 to 0.03 $\text{K}\cdot\text{m}^2/\text{W}$. However, lowest heat gain is found in case of W-shaped rib configuration [29] which decrease 231 to 103 watts in same range of

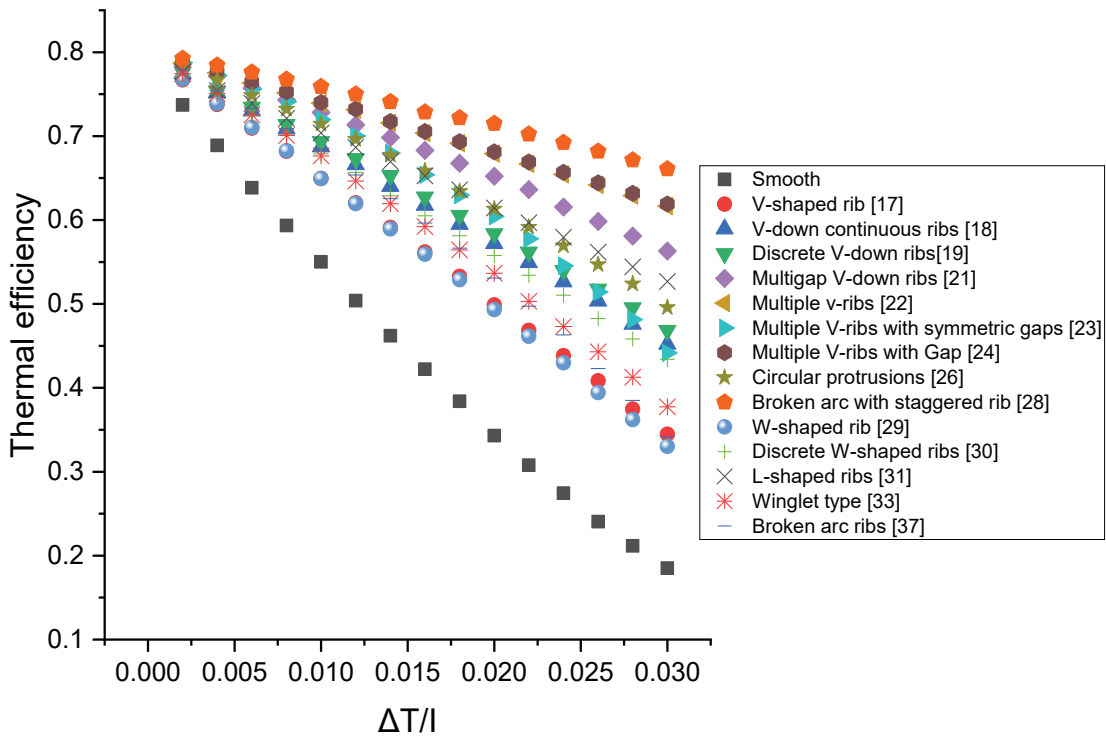


Figure 4. η_{thermal} of roughened duct with respect to $\Delta T/I$.

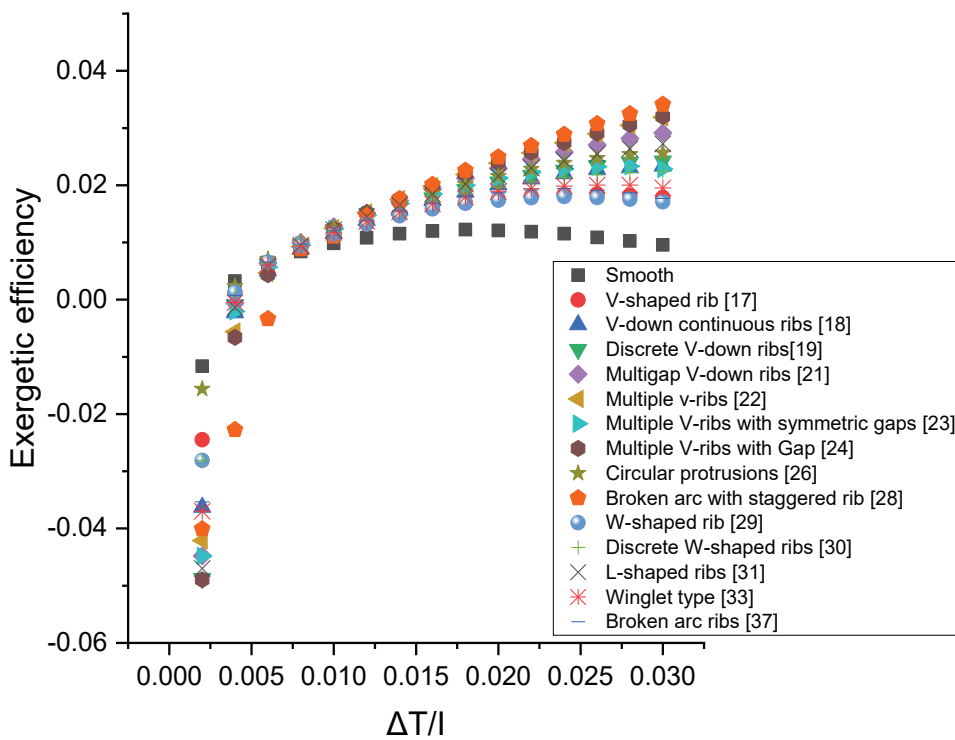


Figure 5. $\eta_{\text{exergetic}}$ of roughened duct with respect to $\Delta T/I$.

temperature rise parameters. Similarly, heat gain in smooth convention absorber have also been plotted for comparison purposes which have lowest heat gain.

The thermal efficiency curves with respect to $\Delta T/I$ and Re have been plotted for distinct type of roughness's in Figure 4. The staggered broken-arc hybrid rib shows consistently higher values of η_{thermal} over the other roughness's and W-shaped ribs shows lower values of η_{thermal} over the other surface. The exergy efficiency curves with respect to $\Delta T/I$ and Re have been plotted for distinct type of roughness's as shown in Figure 5. the value of exergetic efficiency at distinct value of $\Delta T/I$ for different roughness's is shown in table 3. The staggered broken-arc hybrid rib shows consistently higher values of $\eta_{\text{exergetic}}$ over the other roughness's and W-shaped ribs shows lower values of $\eta_{\text{exergetic}}$ over the other surface. The highest value of exergetic efficiency is achieved by all distinct roughnesses at $\Delta T/I$ more than 0.012.

The thermal and exergetic efficiency of the rough surfaces have been compared with the thermal and exergetic efficiency of the smooth surface in the same experimental conditions. It has been found that the optimum performance achieved at $e/D_h = 0.043$, $p/e = 10$, $\alpha = 60^\circ$ and $W/w = 6$. Also, the unique combination of parameters $e/D_h = 0.043$, $p/e = 10$ and $\alpha = 60^\circ$ are observed for best performance.

CONCLUSION

This paper presents a numerical study for predicting the exergy efficiency of SAH having roughened absorber surface. The effects of $\Delta T/I$ on the exergy efficiency were determined. The exergy efficiency of roughened SAH was calculated numerically with the help of developed correlations and the results also compared with conventional SAH under same operating parameters. The conclusions of the study are as follows-

1. The exergetic evaluation of roughened SAH suggest that use of staggered broken-arc shape roughened SAH for Re less than 20,000 and for more than 20,000 conventional smooth plat SAH is suitable.
2. The roughness parameters and flow Re have combined effect on the thermal performance of SAH.
3. At lower value of $\Delta T/I$ the exergy efficiency may be negative.
4. A set of unique combination of parameters $p/e = 10$, $e/D_h = 0.043$ and $\alpha = 60^\circ$ have been observed for best exergetic performance. It is same for all insolation values.
5. The exergy efficiency strongly depends on the Re and $\Delta T/I$.
6. The analysis present in this paper facilitates the researchers to design the absorber plate of SAH by using concept of exergetic efficiency.
7. Hybrid ribs configuration exhibited the highest exergetic efficiencies when temperature rise parameters greater than 0.01 K.m/W, however, smooth duct also showed a significant exergetic efficiency when temperature rise parameters had low values.

NOMENCLATURE

Symbol	Title	Unit
D	Pipe inside diameter (to base of ribs)	m
D_h	Hydraulic diameter of duct	m
e	Roughness height	m
e^+	Roughness Reynolds number	-
e/D_h	Relative roughness height	-
f	Friction factor of roughened surface	-
F_R	Heat removal factor	-
g	Heat transfer roughness function	-
hr	Radiative heat transfer coeff.	W/m ² .K
hc	Convective heat transfer coeff.	W/m ² .K
hw	Wind convective heat transfer coeff.	W/m ² .K
I	Insolation	W/m ²
M	Mass flow rate per unit collector area	Kg/s m ²
Nu	Nusselt number	-
Q_u	Heat gain	W
Q_{e^+}	Heat transfer function	-
R	Momentum transfer roughness function	-
Ra	Rayleigh number	-
Re	Reynolds number	-
St	Stanton number	-
T_a	Ambient temperature	K
T_f	Mean air temperature	K
T_i	Air inlet temperature	K
T_p	Plate temperature	K
T_w	Wall temperature	K
ΔP	Pressure drops	N/m ²
U_o	Overall heat loss coefficient	W/m ² .K
V	Velocity of air in SAH duct	m/s
t_i	Thickness of insulation	mm
t_g	Thickness of glass cover	mm
t_g	Height of collector edge	mm
\dot{U}_b	Back heat loss coefficient	W/m ² .K
U_e	Edge heat loss coefficient	W/m ² .K
U_t	Top heat loss coefficient	W/m ² .K
V	Air velocity	m/s
V_w	Wind Speed	m/s
α	Angle of attack	degree
α'	Arc angle	degree
β'	Thermal expansion coefficient of air	1/K
ϵ_g	Glass cover emissivity	-
ϵ_p	Absorber plate emissivity	-
ν	Kinematic viscosity,	m ² /s
τ	Transmissivity	-
σ	Stefan-Boltzmann constant,	W/m ² .K ⁴
η	Thermal efficiency	-

AUTHORSHIP CONTRIBUTIONS

Authors equally contributed to this work.

DATA AVAILABILITY STATEMENT

The authors confirm that the data that supports the findings of this study are available within the article. Raw data that support the finding of this study are available from the corresponding author, upon reasonable request.

CONFLICT OF INTEREST

The author declared no potential conflicts of interest with respect to the research, authorship, and/or publication of this article.

ETHICS

There are no ethical issues with the publication of this manuscript.

REFERENCES

- [1] Singh I, Singh S. A review of artificial roughness geometries employed in solar air heaters. *Renew Sustain Energy Rev* 2018;92:405–425. [\[CrossRef\]](#)
- [2] Sukhatme K, Sukhatme SP. *Principles of Thermal Collection and Storage*. 2nd ed. India: Tata McGraw-Hill Education, 1996.
- [3] Alam T, Kim MH. Performance improvement of double-pass solar air heater--A state of art of review. *Renew Sustain Energy Rev* 2017;79:779–793. [\[CrossRef\]](#)
- [4] Alam T, Kim MH. A comprehensive review on single phase heat transfer enhancement techniques in heat exchanger applications. *Renew Sustain Energy Rev* 2018;81:813–839. [\[CrossRef\]](#)
- [5] Singh Bisht V, Kumar Patil A, Gupta A. Review and performance evaluation of roughened solar air heaters. *Renew Sustain Energy Rev* 2018;81:954–977. [\[CrossRef\]](#)
- [6] Alam T, Kim MH. A critical review on artificial roughness provided in rectangular solar air heater duct. *Renew Sustain Energy Rev* 2017;69:387–400. [\[CrossRef\]](#)
- [7] Patil AK, Saini JS, Kumar K. A comprehensive review on roughness geometries and investigation techniques used in artificially roughened solar air heaters. *Int J Renew Energy Res* 2012;2:1–15.
- [8] Yadav S, Kaushal M. Exergetic performance evaluation of solar air heater having arc shape oriented protrusions as roughness element. *Sol Energy* 2014;105:181–189. [\[CrossRef\]](#)
- [9] Singh S, Chander S, Saini JS. Exergy based analysis of solar air heater having discrete V-down rib roughness on absorber plate. *Energy* 2012;37:749–758. [\[CrossRef\]](#)
- [10] Bejan A. *Advanced engineering thermodynamics*. 1st ed. New York: Wiley; 1988.
- [11] Lior N, Zhang N. Energy, exergy, and second law performance criteria. *Energy* 2007;32:281–296. [\[CrossRef\]](#)
- [12] Kumar A, Layek A. Energetic and exergetic based performance evaluation of solar air heater having winglet type roughness on absorber surface. *Sol Energy Mater Sol Cells* 2021;230:111147. [\[CrossRef\]](#)
- [13] Gupta MK, Kaushik SC. Exergetic performance evaluation and parametric studies of solar air heater. *Energy* 2008;33:1691–1702. [\[CrossRef\]](#)
- [14] Gupta MK, Kaushik SC. Performance evaluation of solar air heater for various artificial roughness geometries based on energy, effective and exergy efficiencies. *Renew Energy* 2009;34:465e76. [\[CrossRef\]](#)
- [15] Gupta MK, Kaushik SC. Performance evaluation of solar air heater having expanded metal mesh as artificial roughness on absorber plate. *Int J Therm Sci* 2009;48:1007–1016. [\[CrossRef\]](#)
- [16] Layek A, Saini JS, Solanki SC. Second law optimization of a solar air heater having chamfered rib-groove roughness on absorber plate. *Renew Energy* 2007;32:1967–1980. [\[CrossRef\]](#)
- [17] Ebrahim-Momin AM, Saini JS, Solanki SC. Heat transfer and friction in solar air heater duct with V-shaped rib roughness on absorber plate. *Int J Heat Mass Transf* 2002;45:3383–3396. [\[CrossRef\]](#)
- [18] Istanto T, Danardono D, Yaningsih I, Wijayanta AT. Experimental study of heat transfer enhancement in solar air heater with different angle of attack of V-down continuous ribs. *AIP Conf Proc* 2016;1737:060002. [\[CrossRef\]](#)
- [19] Singh S, Chander S, Saini JS. Heat transfer and friction factor correlations of solar air heater ducts artificially roughened with discrete V-down ribs. *Energy* 2011;36:5053–5064. [\[CrossRef\]](#)
- [20] Singh S, Chander S, Saini JS. Thermal and effective efficiency based analysis of discrete V-down rib-roughened solar air heaters. *J Renew Sustain Energy* 2011;3:23107. [\[CrossRef\]](#)
- [21] Deo NS, Chander S, Saini JS. Performance analysis of solar air heater duct roughened with multigap V-down ribs combined with staggered ribs. *Renew Energy* 2016;91:484–500. [\[CrossRef\]](#)
- [22] Hans VS, Saini RP, Saini JS. Heat transfer and friction factor correlations for a solar air heater duct roughened artificially with multiple v-ribs. *Sol Energy* 2010;84:898–911. [\[CrossRef\]](#)
- [23] Singh A, Kumar R, Singh P, Goel V. Solar air heater having multiple V-ribs with Multiple-Symmetric gaps as roughness elements on Absorber-Plate : A parametric study. *Sustain Energy Technol Assessments* 2021;48:101559. [\[CrossRef\]](#)
- [24] Kumar A, Saini RP, Saini JS. Experimental investigations on thermo-hydraulic performance due to flow- attack- angle in multiple V-ribs with gap in a rectangular duct of solar air heaters. *J Sustain Energy Environ* 2013;4:1–7.
- [25] Kumar A, Saini RP, Saini JS. Development of correlations for Nusselt number and friction factor for solar air heater with roughened duct having multi v-shaped with gap rib as artificial roughness. *Renew Energy* 2013;58:151–163. [\[CrossRef\]](#)
- [26] Yadav S, Kaushal M, Varun, Siddhartha. Nusselt number and friction factor correlations for solar air heater duct having protrusions as roughness elements on absorber plate. *Exp Therm Fluid Sci* 2013;44:34–41. [\[CrossRef\]](#)

- [27] Gill RS, Hans VS, Singh S. Investigations on thermo-hydraulic performance of broken arc rib in a rectangular duct of solar air heater. *Int Commun Heat Mass Transf* 2017;88:20–27. [\[CrossRef\]](#)
- [28] Gill RS, Hans VS, Singh RP. Optimization of artificial roughness parameters in a solar air heater duct roughened with hybrid ribs. *Appl Therm Eng* 2021;191:116871. [\[CrossRef\]](#)
- [29] Lanjewar AM, Bhagoria JL, Sarviya RM, Lanjewar AM, Bhagoria L. Performance analysis of W-shaped rib roughened solar air heater. *J Renew Sustain Energy* 2011;3:043110. [\[CrossRef\]](#)
- [30] Kumar A, Bhagoria JL, Sarviya RM. Heat transfer and friction correlations for artificially roughened solar air heater duct with discrete W-shaped ribs. *Energy Convers Manag* 2009;50:2106–2117. [\[CrossRef\]](#)
- [31] Gawande VB, Dhoble AS, Zodpe DB, Chamoli S. Experimental and CFD investigation of convection heat transfer in solar air heater with reverse L-shaped ribs. *Sol Energy* 2016;131:275–295. [\[CrossRef\]](#)
- [32] Kumar A, Layek A. Nusselt number and friction characteristics of a solar air heater that has a winglet type vortex generator in the absorber surface. *Exp Therm Fluid Sci* 2020;119:110204. [\[CrossRef\]](#)
- [33] Kumar A, Layek A. Nusselt number and friction factor correlation of solar air heater having winglet type vortex generator over absorber plate. *Sol Energy* 2020;205:334–348. [\[CrossRef\]](#)
- [34] Patel YM, Jain SV, Lakhera VJ. Thermo-hydraulic performance analysis of a solar air heater roughened with reverse NACA profile ribs. *Appl Therm Eng* 2020;170:114940. [\[CrossRef\]](#)
- [35] Kumar A, Layek A. Energetic and exergetic performance evaluation of solar air heater with twisted rib roughness on absorber plate. *J Clean Prod* 2019; 232:617–628. [\[CrossRef\]](#)
- [36] Promvong P, Khanoknaiyakarn C, Sripattanapipat S, Skullong S. Heat transfer in solar air duct with multi-V-ribbed absorber and grooved back-plate. *Chem Eng Res Des* 2021;168:84–95. [\[CrossRef\]](#)
- [37] Hans VS, Gill RS, Singh S. Heat transfer and friction factor correlations for a solar air heater duct roughened artificially with broken arc ribs. *Exp Therm Fluid Sci* 2016; 80:77–89. [\[CrossRef\]](#)
- [38] Al-Dulaimi MJ, Kareem FA, Hamad FA. Numerical investigation of the heat transfer enhancement inside a square duct with rectangular vortex generators. *J Therm Eng* 2022;8:1–13. [\[CrossRef\]](#)
- [39] Afsharpanah F, Sheshpoli AZ, Pakzad K, Ajarostaghi SSM. Numerical investigation of non-uniform heat transfer enhancement in parabolic trough solar collectors using dual modified twisted-tape inserts. *J Therm Eng* 2021;7:133–147. [\[CrossRef\]](#)
- [40] Sachdev T, Gaba VK, Tiwari AK. Comparative thermal analysis of applications using novel solar air heater with U-shaped longitudinal fins: Suitable for coastal regions. *J Therm Eng* 2021;7:1174–1183. [\[CrossRef\]](#)
- [41] Panda S, Kumar R. A review on effect of various artificial roughness on heat transfer enhancement in a channel flow. *J Therm Eng* 2021;7:1267–1301. [\[CrossRef\]](#)
- [42] Bharadwaj G, Sharma K, Mausam K. Factors influencing the performance of solar air heater (SAH) having artificial coarseness: A review. *J Therm Eng* 2021;7:1556–1576. [\[CrossRef\]](#)
- [43] Duffie JA, Beckman WA. *Solar engineering thermal processes*. 4th ed. New York: John Wiley; 1991.
- [44] Cortes A, Piacentini R. Improvement of the efficiency of a bare solar collector by means of turbulence promoters. *Appl Energy* 1990;36:253–261. [\[CrossRef\]](#)
- [45] Kreith F. *Mechanical Engineering Handbook*. Boca Raton: CRC Press; 1999. [\[CrossRef\]](#)
- [46] Bhushan B, Singh R. Thermal and thermohydraulic performance of roughened solar air heater having protruded absorber plate. *Sol Energy* 2012;86:3388–3396. [\[CrossRef\]](#)
- [47] Hans V. Heat transfer and friction factor characteristics of multiple rib roughened solar air heater. PhD Thesis. India: Indian Institute of Technology Roorkee; 2010.
- [48] Yadav S, Kaushal M. Exergetic performance evaluation of solar air heater having arc shape-oriented protrusions as roughness element. *Sol Energy* 2014;105:181–189. [\[CrossRef\]](#)
- [49] Alam T, Meena CS, Balam NB, Kumar A, Cozzolino R. Thermo-hydraulic performance characteristics and optimization of protrusion rib roughness in solar air heater. *Energies* 2021;14:3159. [\[CrossRef\]](#)
- [50] Sahu MK, Prasad RK. Exergy based performance evaluation of solar air heater with arc-shaped wire roughened absorber plate. *Renew Energy* 2016;96:233–243. [\[CrossRef\]](#)
- [51] Chamoli S, Thakur NS. Performance evaluation of solar air heater having V-down perforated baffles on the absorber plate. *J Renew Sustain Energy* 2013;5:063107. [\[CrossRef\]](#)
- [52] Karmveer, Gupta NK, Alam T, Cozzolino R, Bella G. A descriptive review to access the most suitable rib's configuration of roughness for the maximum performance of solar air heater. *Energies* 2022;15:2800. [\[CrossRef\]](#)
- [53] Karmveer, Gupta NK, Siddiqui MIH, Dobrota D, Alam T, Ali MA, et al. The effect of roughness in absorbing materials on solar air heater performance. *Materials* 2022;15:3088. [\[CrossRef\]](#)
- [54] Altfeld K, Leiner W, Fiebig M. Second law optimization of flat-plate solar air heaters, part I: the concept of net exergy flow and the modelling of solar air heaters. *Sol Energy* 1988;41:127–132. [\[CrossRef\]](#)